

Complementary probes of Bilinear RPV SUSY models with a wino-like LSP via Neutrino Oscillation and LHC

Arghya Choudhury,^a Arpita Mondal^{a,b}

^a*Department of Physics, Indian Institute of Technology Patna, Bihar - 801106, India*

^b*Laboratoire de Physique Subatomique et de Cosmologie (LPSC), Université Grenoble-Alpes, CNRS/IN2P3, 53 Avenue des Martyrs, F-38026 Grenoble, France*

E-mail: arghya@iitp.ac.in, arpita.mondal@lpsc.in2p3.fr

ABSTRACT: In this work, we explore the bilinear R-parity violating Supersymmetry model's parameter space by performing a Markov Chain Monte Carlo scan with neutrino oscillation data, Higgs mass and its coupling strengths, and flavor observables such as B -hadron decay branching ratios. From the allowed parameter space, we analyze the decay patterns of wino-like lighter charginos and lightest neutralinos and demonstrate how the branching ratios to different neutrino and charged lepton flavors depend on the neutrino mass hierarchy. Furthermore, we investigate the impact of current LHC bounds and projected future sensitivities from trilepton resonance searches on the allowed parameter space. We show that considering the branching ratio $\text{Br}(\tilde{\chi}_1^\pm \rightarrow Zl^\pm; l = e, \mu, \tau) \sim 23\%$, obtained at the best-fit point, the wino-like mass degenerate $\tilde{\chi}_1^\pm/\tilde{\chi}_1^0$ are excluded upto 565 GeV from LHC Run-II data. The projected exclusion reach with a similar branching ratio at High-Luminosity LHC (HL-LHC) is around 950 GeV. For a simplified scenario where $\tilde{\chi}_1^\pm/\tilde{\chi}_1^0$ decays via a Z boson with branching ratios of 1%, 50%, and 100%, wino masses can be excluded up to approximately 600 GeV, 1185 GeV, and 1350 GeV respectively. Our analysis shows that the HL-LHC can probe a significant portion of the 1σ allowed parameter space by neutrino oscillation measurements and other experimental constraints.

Contents

1	Introduction	1
2	Neutrino mass generation and observable	4
3	Parameter space and analysis details	5
4	Results and Discussions	7
4.1	Normal Hierarchy	7
4.1.1	Revisiting the LHC trilepton resonance search	11
4.1.2	Prospects of Trilepton Resonance Search at the HL-LHC	14
4.2	Inverted Hierarchy: Brief Discussion	15
5	Conclusion	18
6	Acknowledgement	19
	Bibliography	19

1 Introduction

The discovery of neutrino oscillations [1–7] has undoubtedly established that neutrinos have mass and undergo flavor mixing. These findings present a fundamental challenge to the Standard Model (SM) [8–10], which assumes neutrinos to be massless. Understanding the origin and smallness of neutrino masses, as well as their mixing patterns, remains one of the central questions and a key driver for exploring physics beyond the Standard Model (BSM). Supersymmetry (SUSY) [11–13] provides an elegant solution to several longstanding issues in particle physics, such as

the hierarchy problem [14, 15] and gauge coupling unification [16–18], existence of Dark Matter (DM) [19–22] in the form of lightest supersymmetric particle (LSP), etc. Still, the Minimal Supersymmetric Standard Model (MSSM) cannot explain the existence of non-zero neutrino masses and their mixing. But it can naturally offer a mechanism to generate neutrino masses when extended to include R-parity violation (RPV) [23–43]. Neutrino masses and mixing are commonly generated by seesaw mechanisms, which implement the dimension-5 Weinberg operator [44, 45] by extending the SM with particles like singlet fermions (Type-I), scalar triplets (Type-II), or fermionic triplets (Type-III) [46–50]. Alternatively, RPV MSSM provides a framework to explain neutrino oscillations without invoking the Weinberg operator, although the operator can still be generated from RPV terms at low energies.

The superpotential of the RPV MSSM [23–25] is given by

$$W_{\mathcal{K}_p} = \epsilon_i \hat{L}_i \hat{H}_u + \frac{1}{2} \lambda_{ijk} \hat{L}_i \hat{L}_j \hat{E}_k^c + \lambda'_{ijk} \hat{L}_i \hat{Q}_j \hat{D}_k^c + \frac{1}{2} \lambda''_{ijk} \hat{U}_i^c \hat{U}_j^c \hat{D}_k^c. \quad (1.1)$$

Here, the first three terms refer to the lepton number violation, and the last term correspond to the baryon number violation. \hat{L}_i (\hat{E}_k) represents the left-handed (right-handed) lepton supermultiplet, and \hat{H}_u corresponds to the up-type Higgs supermultiplet. Likewise, \hat{Q}_j , \hat{U}_j , and \hat{D}_k denote the left-handed quark doublet, the right-handed up-type quark singlet, and the right-handed down-type quark singlet supermultiplets, respectively. ϵ_i refers to the bilinear coupling, which shows the coupling between the neutrino and the Higgsinos. The trilinear coupling λ_{ijk} (λ'_{ijk}) shows coupling between lepton, slepton, and neutrino (quark, squark, and neutrino). Similarly, the baryon number violating coupling λ''_{ijk} reflects the coupling between squark and quarks. All three lepton number violating terms contribute to the generation of the neutrino masses. However, only the bilinear RPV (**brPV**) term can generate neutrino mass at both the tree-level and loop-level [36, 51, 52]. The other two terms, associated with λ and λ' , couplings generate neutrino masses exclusively at the loop-level¹. Bilinear RPV term can exist independently or be generated from trilinear terms via renormalization group evolution, and vice versa [54–56]. So, in this work, we focus on the **brPV** model to explain the neutrino oscillation data.

There are a few existing studies in the literature that explore neutrino data with **brPV** model [57–67]. In a recent study [66], the parameter space of the **brPV** model was examined in the context of neutrino oscillation data, focusing on a bino-type neutralino LSP and a wino-type chargino NLSP. In this work, however, we consider both the lightest neutralino and lighter chargino to be wino-type, where both decay directly into different bosons (W^\pm , Z , and h) and leptons or neutrinos [68–70]. Such

¹In a recent work [53], authors have explicitly explored the parameter space of trilinear lepton number violating model in the context of neutrino oscillation data for bino and stop LSP and shown the possible collider signatures at the Large Hadron Collider (LHC).

signals have been investigated by the ATLAS Collaboration at the LHC using Run-II data [71], providing limits on wino-type lighter chargino ($\tilde{\chi}_1^\pm$) or lightest neutralino ($\tilde{\chi}_1^0$) masses based on the branching ratio to Z boson. This branching fraction to different flavors of neutrinos or leptons highly depends on the neutrino mass hierarchy [68–70]. So, we explore this scenario, extract the allowed parameter space, and study the impact of neutrino data on the decay branching ratios of charginos and neutralinos. In addition to the neutrino oscillation data, we also consider Higgs data, including the Higgs boson mass and its coupling strengths with various SM particles. Furthermore, flavor physics observables, such as b -hadron decay branching ratios, are included in our analysis. Given the large number of parameters in the bRPV model and the extensive set of observables considered, we employ the Markov Chain Monte Carlo (MCMC) method to thoroughly scan the parameter space and identify the allowed regions that satisfy all constraints. Additionally, during the parameter space scanning, we incorporate the latest exclusion limits on sparticle masses.

The strongly interacting (colored) sparticles, namely the squarks and gluinos, are excluded up to masses of a few TeV by the current LHC data [72, 73]. In contrast, the constraints on the electroweakino and slepton sectors are comparatively weaker in both R-parity conserving (RPC) and R-parity violating (RPV) scenarios [72, 73]. In RPC scenarios, light electroweakinos and sleptons play a crucial role in dark matter phenomenology, and several phenomenological analyses have addressed this issue along with the interpretations of LHC limits for various production and decay modes [74–89]. These light sparticles in the RPV scenarios have more diverse final states depending on the non-zero RPV couplings and the phenomenological implications have been studied in refs.[25, 90–99]. However the collider phenomenology with RPV SUSY models is relatively less explored. It is worth mentioning that the electroweakinos, particularly the charginos and neutralinos, play a direct role in neutrino mass generation in the present framework. Motivated by these considerations, we also explore the collider implications of the model in the context of trilepton resonance search at the Large Hadron Collider (LHC). Using the Run-II results of trilepton resonance search provided by the ATLAS Collaboration [71] with an integrated luminosity $\mathcal{L} = 139 \text{ fb}^{-1}$, we reinterpret the exclusion limits on wino-like $\tilde{\chi}_1^\pm$ or $\tilde{\chi}_1^0$ mass as a function of its branching ratio to the Z boson. We compare these limits related to its branching ratios predicted from the neutrino sector and show that the parameter space allowed by neutrino oscillation data, along with other data, remains consistent with current LHC constraints. Furthermore, we estimate the future sensitivity of the High-Luminosity LHC (HL-LHC) with $\mathcal{L} = 3 \text{ ab}^{-1}$ and determine the projected exclusion reach for the chargino/neutralino mass as a function of its decay branching ratio to the Z boson.

The paper is organized as follows. In Section 2, we discuss the generation of

neutrino masses and mixing angles in the **brPV** model, along with the observables considered in our analysis. The recent collider limits on sparticles, the parameter space, and the details of the MCMC analysis are presented in Section 3. Our results are shown and explained in Section 4. Finally, we conclude in Section 5.

2 Neutrino mass generation and observable

The lagrangian from the superpotential of the **brPV** and the soft term in the lagrangian [23, 24, 26] can be written as

$$\mathcal{L} = \epsilon_i \left(\tilde{H}_u^0 \nu_{iL} - \tilde{H}_u^+ l_{iL} \right) + \text{h.c.}; \quad \mathcal{L}_{\text{soft}} = B_i \left(\tilde{\nu}_i H_u^0 - \tilde{l}_i^- H_u^+ \right) + \text{h.c.}, \quad (2.1)$$

where ϵ_i represents the coupling between neutrino (ν_i) and Higgsino (\tilde{H}_u^0) and lepton (l_i) and Higgsino (\tilde{H}_u^+). Similarly, the soft coupling B_i refers to the coupling between sneutrino ($\tilde{\nu}$) and Higgs (H_u^0) and slepton (\tilde{l}) and Higgs (H_u^+). Because of the coupling of up-type Higgsinos with neutrinos, neutrino mass can be generated at the tree-level. At this level, the neutralino-neutrino mass matrix becomes a 7×7 structure in the basis [26, 27, 51, 56, 66] ($\tilde{B} \tilde{W}_3 \tilde{H}_d^0 \tilde{H}_u^0 \nu_e \nu_\mu \nu_\tau$), where \tilde{B} and \tilde{W}_3 refer to the bino and wino states, respectively. Additionally, couplings between different Higgs states (h, H, A) and sneutrinos lead to sneutrino mass splitting, which contributes to neutrino mass generation through loop-level processes [36]. These mechanisms are illustrated in Figure 1, showcasing neutrino mass generation via the tree-level process (left), BB -loop process (middle), and ϵB -loop process (right).

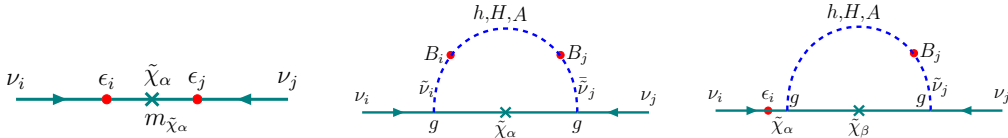


Figure 1: Neutrino mass generation mechanisms: tree-level (left), BB -loop (middle), and ϵB -loop (right) [66].

Combining these three contributions one can write the neutrino mass as [24, 51]

$$[m_\nu]_{ij} = X_T \epsilon_i \epsilon_j \sin^2 \zeta + C_{ij} B_i B_j + (C'_{ij} \epsilon_i B_j + i \leftrightarrow j), \quad (2.2)$$

where first, second, and third term represent the tree-level, BB -loop, and ϵB -loop contribution respectively. ζ shows the alignment between ϵ_i parameters and sneutrino vev (v_i) [30, 56, 100, 101]. The definition of X_T is given by [51, 52]

$$X_T = \frac{m_Z^2 m_{\tilde{\gamma}} \cos^2 \beta}{\mu (m_Z^2 m_{\tilde{\gamma}} \sin 2\beta - M_1 M_2 \mu)} \quad (2.3)$$

where $m_{\tilde{\gamma}} \equiv \cos^2 \theta_w M_1 + \sin^2 \theta_w M_2$. Assuming all the neutrino masses at the EWSB scale (\tilde{m}), the approximate neutrino masses at the tree-level and from the two loop-level processes are expressed as [25, 52, 66]:

$$[m_\nu]_{ij}^{\epsilon\epsilon} \sim \frac{\cos^2 \beta}{\tilde{m}} \epsilon_i \epsilon_j \sin^2 \zeta, \quad (2.4)$$

$$[m_\nu]_{ij}^{BB} \sim \frac{g^2}{64\pi^2 \cos^2 \beta} \frac{B_i B_j}{\tilde{m}^3} \epsilon_H, \quad (2.5)$$

$$[m_\nu]_{ij}^{\epsilon B} \sim \frac{g^2}{64\pi^2 \cos \beta} \frac{\epsilon_i B_j + \epsilon_j B_i}{\tilde{m}^2} \epsilon'_H, \quad (2.6)$$

where \tilde{m} represents the electroweak symmetry breaking scale, and $\sin^2 \zeta$ corresponds to the alignment between the bRPV coupling (ϵ) and the sneutrino vacuum expectation value (v) [30, 56, 100, 101]. The factors ϵ_H and ϵ'_H quantify the cancellation effects of different Higgs states in the BB -loop and ϵB -loop, respectively [28, 51, 52]. It is noteworthy that at the tree-level, only a single neutrino, the heaviest mass eigenstate, acquires a significant mass.

Now using this bRPV model, we attempt to satisfy the neutrino oscillation parameters [102] corresponding to both neutrino mass orderings: the Normal Hierarchy (NH) with $m_{\nu_3} > m_{\nu_2} > m_{\nu_1}$ and Inverted Hierarchy (IH) with $m_{\nu_2} > m_{\nu_1} > m_{\nu_3}$. Each scenario includes two mass square splittings (Δm_{21}^2 and $|\Delta m_{31}^2|$) and three mixing angles (θ_{13} , θ_{12} , and θ_{23}). It should be noted that we have not considered the CP-violating phase (δ_{CP}) since adding this phase does not alter the parameter space [66]. We have considered the constraint on the neutrino masses sum coming from the cosmological data [102]. Additionally, we incorporate the Higgs data, such as the Higgs boson mass [103] and its coupling with various Standard Model particles like Z , W , b , τ , μ , t , γ given by CMS Collaboration [104]. Furthermore, we take into account the branching ratios of b -hadron decays, including $\mathcal{B}r(B_s \rightarrow \mu^+ \mu^-)$ [105] and $\mathcal{B}r(B \rightarrow X_s \gamma)$ [106]. The values of these observables, along with the prior on neutrino masses sum under consideration, are listed in Table 1.

3 Parameter space and analysis details

In this analysis, we have considered a bRPV model with wino-type LSP. In this model, the lightest neutralino ($\tilde{\chi}_1^0$) and the lighter chargino ($\tilde{\chi}_1^\pm$) are almost mass degenerate. The strongest limits on sparticle masses in the RPV scenarios mainly come from LLE (λ) type couplings. Using the Run-II data, the ATLAS and CMS Collaborations have excluded gluino, light squarks, stop, slepton, and chargino upto 2.5 TeV [108], 1.6 TeV [109], 1.9 TeV [110], 1.2 TeV [108], and 1.6 TeV [108] respectively. However, the ATLAS Collaboration has searched for winos and Higgsinos in the bRPV scenario.

Observable	Best-fit $^{+1\sigma}_{-1\sigma}$		Observable	Best-fit $^{+1\sigma}_{-1\sigma}$	Observable	Best-fit $^{+1\sigma}_{-1\sigma}$
	NH	IH				
Δm_{21}^2 [10^{-5} eV 2]	$7.50^{+0.22}_{-0.20}$	$7.50^{+0.22}_{-0.20}$	m_h [GeV]	125^{+3}_{-3}	κ_μ	$0.92^{+0.55}_{-0.87}$
$ \Delta m_{31}^2 $ [10^{-3} eV 2]	$2.55^{+0.02}_{-0.03}$	$2.45^{+0.02}_{-0.03}$	κ_Z	$0.96^{+0.07}_{-0.07}$	κ_t	$1.01^{+0.11}_{-0.11}$
θ_{12} [$^\circ$]	$34.3^{+1.0}_{-1.0}$	$34.3^{+1.0}_{-1.0}$	κ_W	$1.11^{+0.14}_{-0.09}$	κ_γ	$1.01^{+0.09}_{-0.14}$
θ_{13} [$^\circ$]	$8.53^{+0.13}_{-0.12}$	$8.58^{+0.12}_{-0.14}$	κ_b	$1.18^{+0.19}_{-0.27}$	$\mathcal{B}r(B_s \rightarrow \mu^+ \mu^-)$ [10^{-9}]	$3.09^{+0.48}_{-0.44}$
θ_{23} [$^\circ$]	$49.26^{+0.79}_{-0.79}$	$49.46^{+0.60}_{-0.97}$	κ_τ	$0.94^{+0.12}_{-0.12}$	$\mathcal{B}r(B \rightarrow X_s \gamma)$ [10^{-4}]	$3.32^{+0.15}_{-0.15}$
Prior			NH		IH	
Cosmological bound, $\sum_i m_{\nu_i}$			< 0.12 eV		< 0.15 eV	

Table 1: Neutrino observables [102] and the cosmological bound on neutrino masses sum [107] corresponding to Normal Hierarchy (NH) and Inverted Hierarchy (IH), Higgs mass [103], Higgs coupling strength modifiers [104], and b -hadron decay branching ratio [105, 106] best-fit values with their 1σ uncertainties are shown.

Higgsinos in the bRPV model are excluded upto 440 GeV [111], and winos are excluded in the mass range 100-1100 GeV [112, 113] depending on the assumptions of decay branching ratio into different flavors of leptons. The decay channels corresponding to different LSPs for different RPV coupling are discussed in details in the Ref. [25, 93, 96] and all the limits on these SUSY particles coming from RPV couplings are summarized in the Refs. [72, 73].

Parameter	Range/Value	Parameter	Range/Value	Parameter	Range/Value
M_1 [GeV]	3000	$\tan \beta$	1-60	B_i [GeV]	1-5000
M_2 [GeV]	500-2000	M_A [GeV]	3000	A_t [GeV]	-3.5
M_3 [GeV]	3000	v_i [10^{-4} GeV]	0.1-50	$m_{\tilde{q}}$ [GeV]	3000
μ [GeV]	3000	$ \epsilon_i $ [GeV]	0-0.5	$m_{\tilde{l}}$ [GeV]	2000

Table 2: The values of fixed parameters and the range of free parameters are shown here.

To avoid the existing limits, we have fixed gluino and all the squark masses at 3 TeV and the slepton masses at 2 TeV. Also, we have set M_A and A_t at 3 TeV and -3.5 TeV respectively². Also, we have set M_1 and μ both at 3 TeV. Now in this scenario, after fixing these parameters, we have considered 11 free parameters to vary - M_2 , $\tan \beta$, three sneutrino vev (v_i), three bRPV coupling (ϵ_i), and three soft bRPV coupling (B_i). The ranges of these input parameters, along with the values of fixed parameters, are mentioned in the Table 2.

²It may be noted that the most strongest limit on $M_A > 1.5$ TeV (for $\tan \beta < 21$) [114, 115] is obtained from $H/A \rightarrow \tau^+ \tau^-$ search.

We have generated our model using the package **SARAH** [116–118], and to generate the spectrum, we have utilized **SPheno** [119, 120] which uses **FlavorKit**[121] for the calculation of flavor physics observables. To scan the parameter space, we employ the Markov Chain Monte Carlo (MCMC) method using the **emcee** package [122]. The MCMC algorithm samples the parameter space according to the likelihood function $\mathcal{L} \propto e^{-\frac{\chi^2}{2}}$ thereby identifying both the maximum-likelihood (minimum χ^2) point and the surrounding high-likelihood regions. The χ^2 function is defined as $\chi^2 = \sum_{i=1}^{n_{\text{obs}}} \left[\frac{X_i^{\text{obs}} - X_i^{\text{th}}}{\sigma_i} \right]^2$, where X_i^{obs} , X_i^{th} , and σ_i denote the experimentally observed value, theoretically predicted value, and experimental uncertainty of the i -th observable, respectively. In this analysis, we have 15 observables and 11 free parameters, which lead to 4 degrees of freedom (**d.o.f**). To scan the parameter space thoroughly, we use 500 walkers and 400 steps for each walker. To ensure that it does not depend on the initial steps of the sampling, we employ 30% burn-in for our analysis.

4 Results and Discussions

We present results for both the NH and IH scenarios, while the collider prospects are discussed only for the NH case. The results for the IH scenario are briefly summarized in Section 4.2 and compared with those of the NH case.

4.1 Normal Hierarchy

In this section, we consider the Normal Hierarchy scenario, where the third neutrino (ν_3) is the heaviest and the first neutrino (ν_1) is the lightest. In this framework, the minimum χ^2 value is obtained as 3.20 for **d.o.f** = 4. The posterior distributions of the input parameters are shown in Figure 2, where the purple, cyan, and red regions correspond to the 1σ , 2σ , and 3σ confidence intervals, respectively. The best-fit point is indicated by the orange dashed line. The input parameters corresponding to this best-fit point, along with the masses of $\tilde{\chi}_1^\pm$ and $\tilde{\chi}_1^0$ and their decay branching ratios, are shown in Table 3. Based on the relationships of tree-level and two loop-level contributions with $\tan\beta$ shown in Equations 2.2-2.6, we observe that $\tan\beta$ acts as a suppression factor for the tree-level contribution while enhancing the loop-level contributions. Since the heaviest neutrino mass primarily arises from the tree-level contribution and the other two from loop-level contributions, $\tan\beta$ should not be excessively large or small. To get the heaviest neutrino mass from the tree-level, the higher M_2 values are expected which is evident from the relation of X_T with M_2 in Equation 2.3. These arguments are reflected at the best-fit point shown in Table 3. From Figure 2, the 3σ allowed range for $\tan\beta$ and M_2 are approximately 7-20 and 800-1900 GeV respectively. As the third neutrino is the heaviest one, ϵ_3 and ν_3 are

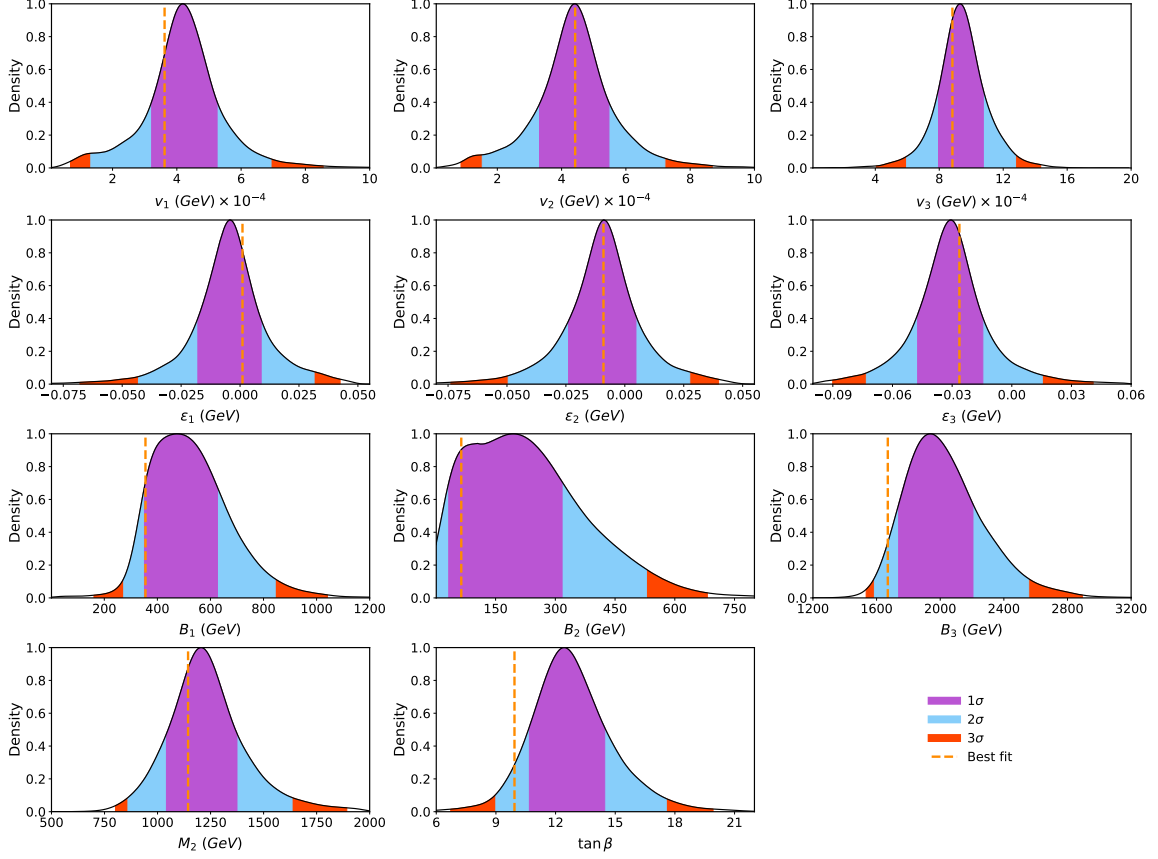


Figure 2: The 1-D posterior distribution of all the input parameter along with 1σ , 2σ and 3σ regions are shown here with purple, cyan and red colors respectively. The best-fit value of each parameter is represented by the dashed orange colored line.

Best-fit Point (BFP)							
Input parameters				$m_{\tilde{\chi}_1^0} = 1191 \text{ GeV}$		$m_{\tilde{\chi}_1^\pm} = 1194 \text{ GeV}$	
Parameter	Value	Parameter	Value	Decay	Br (%)	Decay	Br(%)
M_2 [GeV]	1143.89	ϵ_2 [10^{-3}GeV]	-9.05	$W e$	8.68	$W \nu_\tau$	45.35
$\tan \beta$	9.93	ϵ_3 [10^{-3}GeV]	-26.34	$W \mu$	8.61	$h e$	5.11
v_1 [10^{-4}GeV]	3.61	B_1 [GeV]	355	$W \tau$	28.10	$h \mu$	4.31
v_2 [10^{-4}GeV]	4.42	B_2 [GeV]	64	$h \nu_e$	0.06	$h \tau$	21.92
v_3 [10^{-4}GeV]	8.82	B_3 [GeV]	1670	$h \nu_\mu$	0.17	$Z e$	4.40
ϵ_1 [10^{-3}GeV]	-1.03			$h \nu_\tau$	31.06	$Z \mu$	4.46
$\chi_{\min}^2/\text{d.o.f} = 3.20/4 = 0.8$				$Z \nu_\tau$	23.32	$Z \tau$	14.45

Table 3: The input parameters at the best-fit point, along with the masses of the wino-type lightest neutralino and lighter chargino and their respective decay branching ratios, are presented.

expected to have larger values than other ϵ_i and v_i as shown in Table 3. As the ϵB -loop contribution is significantly suppressed due to the small value of ϵ compared

to the B_i parameters, the B_1 parameter must be larger than the B_2 parameter to make the lightest neutrino mass eigenstate heavy. This is evident from the best-fit values shown in the Table 3.

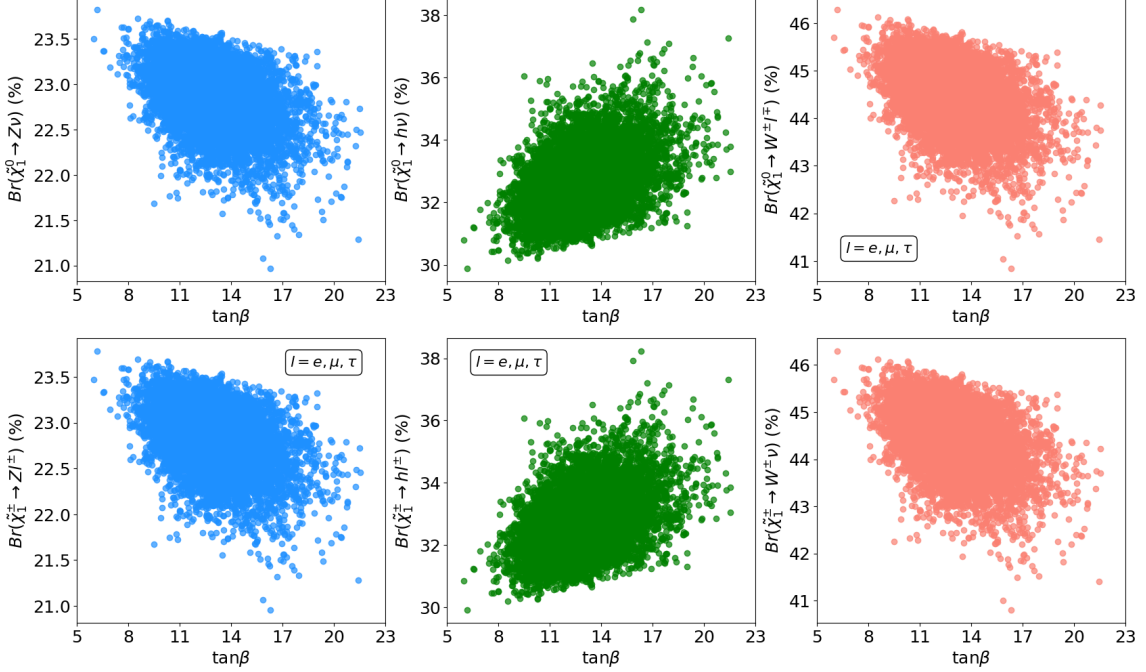


Figure 3: Variations of branching ratios corresponding to the three possible decay channels of a wino-type lightest neutralino ($\tilde{\chi}_1^0$) and a wino-type lighter chargino ($\tilde{\chi}_1^{\pm}$) as functions of $\tan\beta$. The blue, green, and coral points in the upper panel represent $\mathcal{B}r(\tilde{\chi}_1^0 \rightarrow Z\nu)$, $\mathcal{B}r(\tilde{\chi}_1^0 \rightarrow h\nu)$, and $\mathcal{B}r(\tilde{\chi}_1^0 \rightarrow W^{\pm}l^{\mp})$, respectively, with $l = e, \mu, \tau$. Similarly, the blue, green, and coral points in the lower panel correspond to $\mathcal{B}r(\tilde{\chi}_1^{\pm} \rightarrow Zl^{\pm})$, $\mathcal{B}r(\tilde{\chi}_1^{\pm} \rightarrow hl^{\pm})$, and $\mathcal{B}r(\tilde{\chi}_1^{\pm} \rightarrow W^{\pm}\nu)$, respectively.

The ordering of the branching ratios of the $\tilde{\chi}_1^0$ and $\tilde{\chi}_1^{\pm}$ corresponding to different lepton flavors arises from the relative sizes of the parameters which are driven by the neutrino mass hierarchy. Since $m_{\nu_3} > m_{\nu_2} > m_{\nu_1}$, the branching ratios to τ -flavored leptons and neutrinos are the largest. Now we discuss the effect of $\tan\beta$ on the branching ratios of the lighter chargino and the lightest neutralino as shown in Figure 3. We consider the points with $\chi^2 \leq \chi_{\min}^2 + 9.0$, which is the allowed χ^2 value for a 1D parameter space at the 3σ level [123]. From the large dataset of the allowed points, we randomly select only 5% points for further illustration purposes. The relations of the branching ratios of wino-type chargino and neutralino are discussed in Ref. [68–70]. The dependency of $\tan\beta$ and the mass of neutralino is shown in Eqs. (4.3)-(4.5) of Ref. [70] and Eqs. (70)-(74) in Ref. [68]. Additionally, the relationship between mass and $\tan\beta$ to the decay branching ratios for the wino-type chargino is shown in Eqs. (3.7)-(3.9) of Ref. [70]. For the branching ratios to Z and W

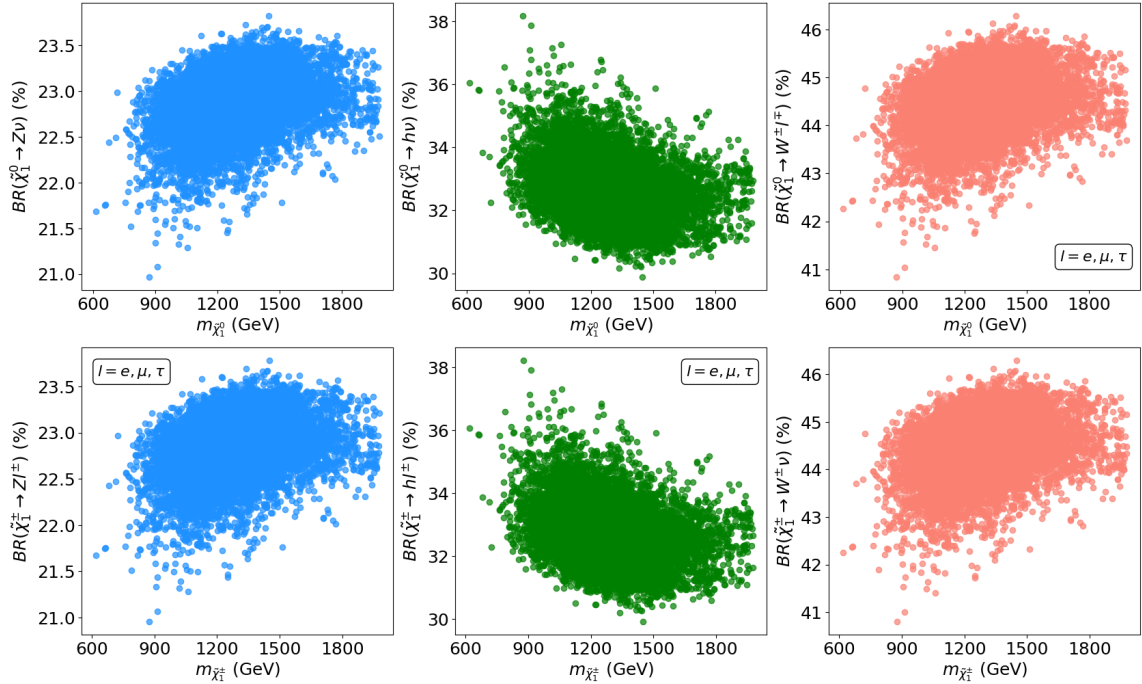


Figure 4: Variations of branching ratios corresponding to the three possible decay channels of $\tilde{\chi}_1^0$ and $\tilde{\chi}_1^\pm$ as functions of their masses. The blue, green, and coral points in the upper panel represent $\mathcal{B}r(\tilde{\chi}_1^0 \rightarrow Z\nu)$, $\mathcal{B}r(\tilde{\chi}_1^0 \rightarrow h\nu)$, and $\mathcal{B}r(\tilde{\chi}_1^0 \rightarrow W^\pm l^\mp)$, respectively, with $l = e, \mu, \tau$. Similarly, the blue, green, and coral points in the lower panel represent $\mathcal{B}r(\tilde{\chi}_1^\pm \rightarrow Zl^\pm)$, $\mathcal{B}r(\tilde{\chi}_1^\pm \rightarrow hl^\pm)$, and $\mathcal{B}r(\tilde{\chi}_1^\pm \rightarrow W^\pm \nu)$, respectively.

bosons $\tan\beta$ acts as a suppression factor ($\propto 1/\sqrt{1 + \tan^2\beta}$), whereas for the Higgs boson, the branching ratio increases with increasing $\tan\beta$ ($\propto \tan^2\beta$) [68–70]. We have also obtained a similar pattern from our analysis, which is reflected in Figure 3. Here we have plotted only the decay modes with a branching fraction $> 1\%$. In Figure 3, $\mathcal{B}r(\tilde{\chi}_1^0 \rightarrow Z\nu/h\nu/W^\pm l^\mp)$ and $\mathcal{B}r(\tilde{\chi}_1^\pm \rightarrow Zl^\pm/hl^\pm/W^\pm \nu)$ are presented via blue, green, and coral colored points, respectively with $l = e, \mu, \tau$. The upper and lower panel correspond to the decay channels of wino-type $\tilde{\chi}_1^0$ and $\tilde{\chi}_1^\pm$ respectively.

Also, we have shown the variation of branching ratios with $m_{\tilde{\chi}_1^0}$ and $m_{\tilde{\chi}_1^\pm}$ in Figure 4. We observe that the branching ratios corresponding to Z and W boson increase with increasing $m_{\tilde{\chi}_1^0}/m_{\tilde{\chi}_1^\pm}$ as reported in previous literature [68, 70]. We now illustrate the effect of the neutrino mass hierarchy on different neutrino and lepton flavors corresponding to various decay channels of the neutralino and chargino in Figure 5. The upper and lower panels represent the decay modes of the lightest neutralino and lighter chargino, respectively. The teal, yellow, and red colors refer to the τ , μ , and e -flavored neutrino and lepton in Figure 5. Since the third neutrino, predominantly τ -flavored, is the heaviest, the bRPV coupling ϵ_3 has the largest value and the decay channels $\tilde{\chi}_1^0 \rightarrow Z\nu_\tau$, $\tilde{\chi}_1^0 \rightarrow h\nu_\tau$ dominate. Similarly, for the chargino,

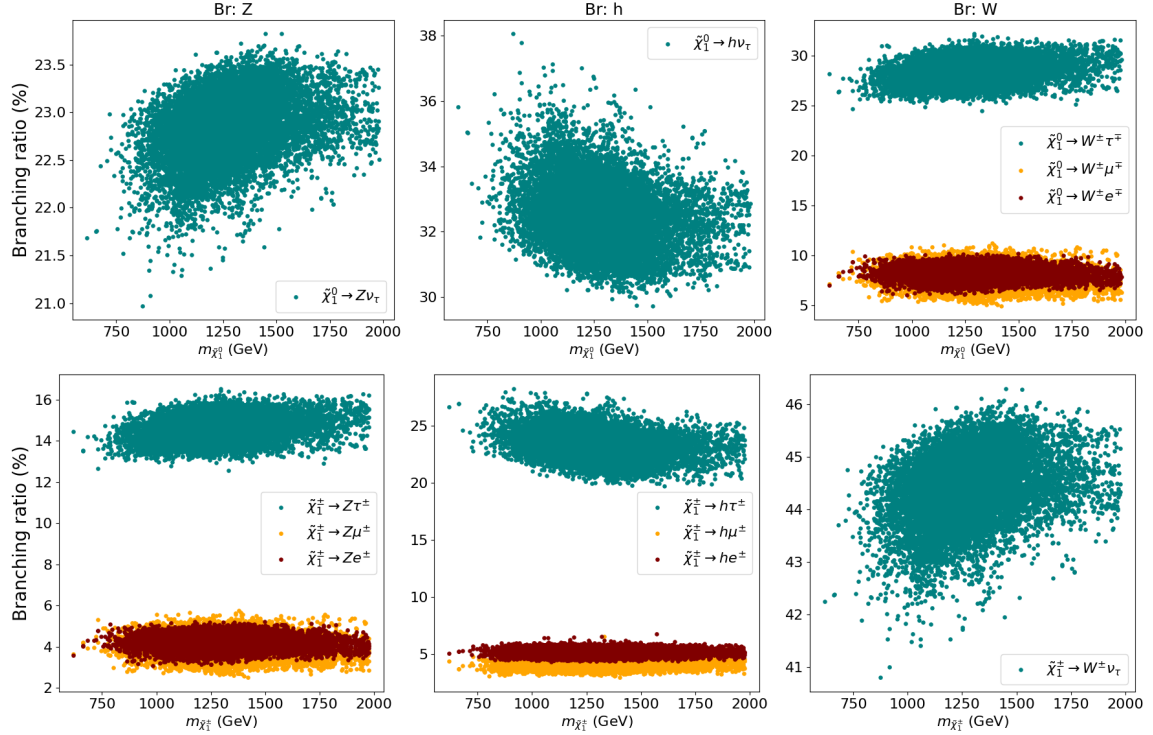


Figure 5: The branching ratios of $\tilde{\chi}_1^0$ and $\tilde{\chi}_1^\pm$ into different lepton flavors are shown. In the upper panel, $\mathcal{B}r(\tilde{\chi}_1^0 \rightarrow Z\nu)$ (left), $\mathcal{B}r(\tilde{\chi}_1^0 \rightarrow h\nu)$ (middle), and $\mathcal{B}r(\tilde{\chi}_1^0 \rightarrow W^\pm l^\mp)$ (right) are presented. In the lower panel, $\mathcal{B}r(\tilde{\chi}_1^\pm \rightarrow Zl^\pm)$ (left), $\mathcal{B}r(\tilde{\chi}_1^\pm \rightarrow hl^\pm)$ (middle), and $\mathcal{B}r(\tilde{\chi}_1^\pm \rightarrow W^\pm\nu)$ (right) are shown. The red, yellow, and teal colors correspond to the first-, second-, and third-generation lepton flavors, respectively.

the $\tilde{\chi}_1^\pm \rightarrow W^\pm\nu_\tau$ decay channel prevails over those involving other neutrino flavors. Furthermore, due to the hierarchy $m_{\nu_3} > m_{\nu_2} > m_{\nu_1}$, the $\tilde{\chi}_1^0 \rightarrow W^\pm\tau^\mp$ decay channel is significantly more prominent than $\tilde{\chi}_1^0 \rightarrow W^\pm\mu^\mp$ and $\tilde{\chi}_1^0 \rightarrow W^\pm e^\mp$, as depicted in the right-hand plot of the upper panel in Figure 5. A similar pattern is observed for the $\tilde{\chi}_1^\pm \rightarrow Z\tau^\pm$ and $\tilde{\chi}_1^\pm \rightarrow h\tau^\pm$ channels, as seen in the left and middle plots of the lower panel in Figure 5, respectively.

4.1.1 Revisiting the LHC trilepton resonance search

ATLAS Collaboration has searched for wino-type $\tilde{\chi}_1^\pm\tilde{\chi}_1^\mp + \tilde{\chi}_1^\pm\tilde{\chi}_1^0$ pair production at $\sqrt{s} = 13$ TeV with $\mathcal{L} = 139$ fb $^{-1}$ [71]. They have looked for trilepton invariant mass spectrum resonance (m_{Zl}), which comes from the wino pair productions where at least one $\tilde{\chi}_1^\pm$ decays to Zl^\pm . The limit on $m(\tilde{\chi}_1^\pm) = m(\tilde{\chi}_1^0)$ ³ was presented as a function of their decay branching ratio to the Z boson. The decay channels con-

³In our case, the masses are not exactly equal but are nearly degenerate and both the particles decay via RPV SUSY interactions.

sidered by ATLAS corresponding to $\tilde{\chi}_1^\pm \tilde{\chi}_1^\mp$ and $\tilde{\chi}_1^\pm \tilde{\chi}_1^0$ are shown in Figure 6. One reconstructed $\tilde{\chi}_1^\pm$ is required in the signal event. Also, events are categorized into three signal regions (SRs: SR31, SR41, and SRFR) depending on the number of leptons and the presence of a second reconstructed W , Z , or h boson from second $\tilde{\chi}_1^\pm/\tilde{\chi}_1^0$ decay. The SRFR region targets events where all decay products are visible and “fully reconstructed”. The SR41 region targets events with four or more leptons and possible missing energy (\cancel{E}_T), while the SR31 region targets events with only three visible leptons and substantial \cancel{E}_T , with at least one neutrino coming from the decay of the second $\tilde{\chi}_1^\pm/\tilde{\chi}_1^0$.

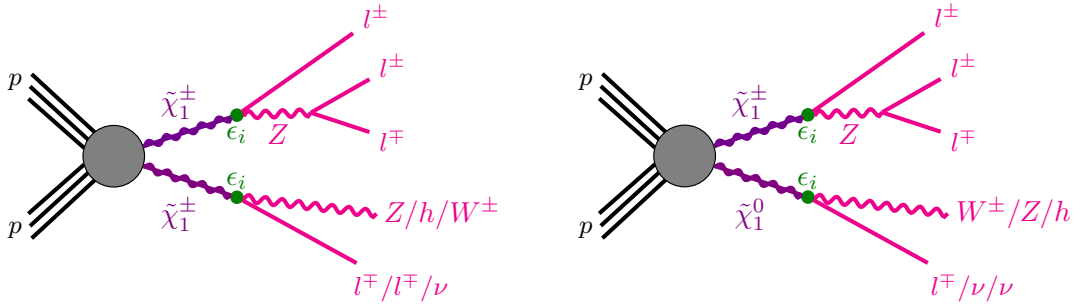


Figure 6: Diagrams of $\tilde{\chi}_1^\pm \tilde{\chi}_1^\mp$ (left) and $\tilde{\chi}_1^\pm \tilde{\chi}_1^0$ (right) productions and decay where at least one $\tilde{\chi}_1^\pm$ decays like $\tilde{\chi}_1^\pm \rightarrow Zl \rightarrow ll$. The other $\tilde{\chi}_1^\pm$ and $\tilde{\chi}_1^0$ decay to W , Z and h boson according to bilinear RPV coupling ϵ .

The ATLAS collaboration has observed that the three signal regions contribute roughly equally to the overall sensitivity of the search, with a minor increase in sensitivity to Higgs boson decays from SRFR offset by a similar increase in sensitivity to W boson decays from SR41 (see Sec 8.2 of the Ref. [71]). In this work, we focus only on the SR31 signal region. First, we validate the result quoted in Table 5 of the auxiliary material provided by the ATLAS collaboration [124], where democratic branching fractions into bosons (W , Z , and Higgs) and leptons (e , μ , and τ) are considered. We generate our signal events using Monte Carlo event generation with MadGraph [125] and do detector simulation with Delphes-3.5.0 [126]. We use the cross-sections at 13 TeV provided by the LHC SUSY working group [127, 128]. Using this set-up, we have validated our results for two mass points, such as 500 GeV and 800 GeV, and the comparison of the two results is shown in the Table 4. We observe an overall good agreement between our simulation and the ATLAS results for the signal yields.

The 95% CL upper limits on number of signal events (S_{obs}^{95}) for each m_{Zl} mass bin of every SR is provided by the ATLAS Collaboration (see Table 4 of Ref [71]). As mentioned above, we consider only SR31 signal region and depending on these given

Selection	500 GeV				800 GeV			
	$\tilde{\chi}_1^\pm \tilde{\chi}_1^0$		$\tilde{\chi}_1^\pm \tilde{\chi}_1^\mp$		$\tilde{\chi}_1^\pm \tilde{\chi}_1^0$		$\tilde{\chi}_1^\pm \tilde{\chi}_1^\mp$	
	ATLAS	Our	ATLAS	Our	ATLAS	Our	ATLAS	Our
Total production ($\sigma \times \mathcal{L}$)	6440	6442	3070	3074	661	661	307	307
≥ 3 signal leptons	82.1	96.56	74.4	96.23	8.89	11.21	7.66	10.65
Z candidate	63.0	46.81	52.0	39.29	6.79	5.44	5.41	5.00
SR3 l assignment	49.5	38.48	30.8	26.69	5.29	4.38	3.16	3.22
$\cancel{E}_T > 150$ GeV	33.4	26.32	15.2	11.93	4.41	3.46	2.03	1.92
$m_T^{\min} > 125$ GeV	25.8	22.49	11.2	9.03	3.65	2.98	1.59	1.60
$\Delta R(b_1, b_2) < 1.5$	24.8	21.26	10.7	8.79	3.54	2.91	1.49	1.58
SR31 $_{e\mu}$	23.4	21.26	10.04	8.79	3.34	2.91	1.41	1.579
SR31 $_e$	11.9	9.95	4.85	4.00	1.71	1.16	0.711	0.676
SR31 $_\mu$	11.5	11.31	5.19	4.79	1.63	1.75	0.703	0.903

Table 4: The signal yields provided by both ATLAS and derived from our simulation corresponding to SR31 signal region at $m_{\tilde{\chi}_1^\pm} = m_{\tilde{\chi}_1^0} = 500$ GeV & 800 GeV.

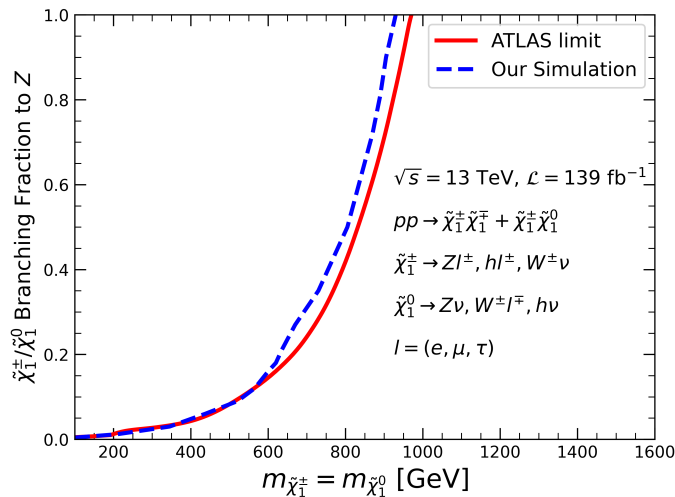


Figure 7: Comparison of the 95% C.L. exclusion limit obtained by ATLAS collaboration with Run-II data [71] and our analysis. The red colored solid line represents the limit obtained by ATLAS and the blue dashed line corresponds to the exclusion reach obtained from our analysis. Here $l = e, \mu, \tau$ is considered and the charged-lepton decays of $\tilde{\chi}_1^\pm/\tilde{\chi}_1^0$ into any leptons with equal probability is imposed here. The sum of the $\tilde{\chi}_1^\pm/\tilde{\chi}_1^0$ branching fractions to W , Z , and h bosons is unity for each point, and the branching fractions to W and h bosons are chosen so as to be equal everywhere.

upper limits, we validate the ATLAS exclusion limit on the $\tilde{\chi}_1^\pm/\tilde{\chi}_1^0$ decay branching fraction to Z and $\tilde{\chi}_1^\pm/\tilde{\chi}_1^0$ mass plane. In Figure 7, we present our validation result where the red solid line represents the ATLAS exclusion limit and the dashed blue

line refers to the exclusion line generated by our simulation. Here, all three flavors of leptons (e, μ, τ) have equal branching ratios. The sum of the $\tilde{\chi}_1^\pm/\tilde{\chi}_1^0$ branching fractions to W, Z , and h bosons is unity for each point, and the branching fractions to W and h bosons are considered to be equal everywhere. From Figure 7, it is evident that our result overlaps at the lower mass region (below ~ 600 GeV) and we also have a nice agreement with the experimental result at higher mass region. The slight difference at the higher mass region may arise because the ATLAS exclusion curve was derived using three signal regions, whereas our result is based on SR31 signal region.

All the above results are for simplified scenarios with some assumptions. In contrast, when we satisfy neutrino oscillation data, the branching ratios to different flavors are generally unequal as discussed in Section 4.1. The masses and the branching ratios of $\tilde{\chi}_1^0$ and $\tilde{\chi}_1^\pm$ at the best-fit point are shown in the Table 3. It is clear from this table that we have a slight (~ 3 GeV) mass difference between $m_{\tilde{\chi}_1^\pm}$ and $m_{\tilde{\chi}_1^0}$, and the branching ratios to Z boson are not equal for $\tilde{\chi}_1^\pm$ and $\tilde{\chi}_1^0$ because of the neutrino oscillation data. At the best-fit point, we have obtained that we can exclude $\tilde{\chi}_1^\pm$ upto ~ 565 GeV with 23% branching ratio to $\tilde{\chi}_1^\pm \rightarrow Ze + Z\mu + Z\tau$ decay.

4.1.2 Prospects of Trilepton Resonance Search at the HL-LHC

We now show the sensitivity reach at the HL-LHC ($\sqrt{s} = 14$ TeV, $\mathcal{L} = 3$ ab $^{-1}$) for wino-type $\tilde{\chi}_1^\pm\tilde{\chi}_1^\mp + \tilde{\chi}_1^\pm\tilde{\chi}_1^0$ pair production. We apply the cuts used for SR3L signal region from ATLAS paper and also assume that the signal selection efficiencies remain unchanged for backgrounds. The predicted exclusion reaches at the HL-LHC are obtained by scaling the background yields from the current ATLAS analysis [71] to the higher luminosity and center-of-mass energy. We assume that the cross sections for the background at 14 TeV will be increased by a factor of 1.2. As similar to 13 TeV results discussed in Section 4.1.1, the signal events are generated using MadGraph [125] and fast detector simulation is done with Delphes-3.5.0 [126]. The NLO+NLL signal production cross-sections at 14 TeV are estimated by Resummino [127, 128]. We find the exclusion mass value by applying the condition

$$\frac{S}{\sqrt{B + (\Delta B \times B)^2}} > 2, \quad (4.1)$$

where S, B , and ΔB are the calculated signal yield, the scaled background yield, and the uncertainty in the background yield, respectively. We consider 10% uncertainty in the background yield here and show the projected exclusion limit at HL-LHC obtained by our simulation in Figure 8. Here, the magenta dashed line represents the HL-LHC projected exclusion limit and the red solid line refers to the ATLAS limit with Run-II data. For branching ratios of $\tilde{\chi}_1^\pm$ decays into a Z boson and a lepton

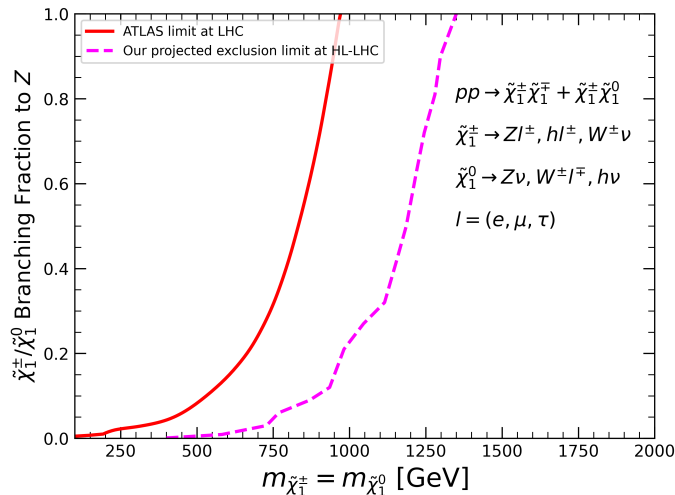


Figure 8: The 95% C.L. projected exclusion limit obtained by our simulation at HL-LHC is shown by magenta-colored dashed line. The red colored solid line represents the limit obtained by ATLAS with Run-II data. Here $l = e, \mu, \tau$ is considered, and the charged-lepton decays of $\tilde{\chi}_1^\pm/\tilde{\chi}_1^0$ into any leptons with equal probability are imposed here. The sum of the $\tilde{\chi}_1^\pm/\tilde{\chi}_1^0$ branching fractions to W , Z , and h bosons is unity for each point, and the branching fractions to W and h bosons are considered to be equal everywhere.

of approximately 1%, 50%, and 100%, wino masses can be excluded up to about 600 GeV, 1185 GeV, and 1350 GeV, respectively. Considering the branching ratio $\text{Br}(\tilde{\chi}_1^\pm \rightarrow Zl^\pm; l = e, \mu, \tau) \sim 23\%$, obtained at the best-fit point, the wino-like mass degenerate $\tilde{\chi}_1^0/\tilde{\chi}_1^\pm$ can be excluded upto 950 GeV at the HL-LHC. Our analysis shows that the HL-LHC can probe a significant portion of 1σ allowed parameter space (see the distribution of M_2 shown in Figure 2) by neutrino oscillation measurements and other experimental constraints.

4.2 Inverted Hierarchy: Brief Discussion

We perform a similar analysis for the IH case where the second neutrino mass eigenstate is the heaviest one and the third neutrino mass eigenstate is the lightest one. We follow the same procedure for IH also as considered for the NH scenario and we present the allowed parameter space in Figure 9. The allowed region of parameter space is significantly smaller compared to the NH scenario, which arises due to the structure of the neutrino mass hierarchy. This hierarchy is also reflected in the best-fit and allowed values of the model parameters as shown in Table 5. As mentioned above, the second neutrino state is the heaviest one and it has an almost equal admixture of all the three neutrino flavors. So, the contribution from tree-level

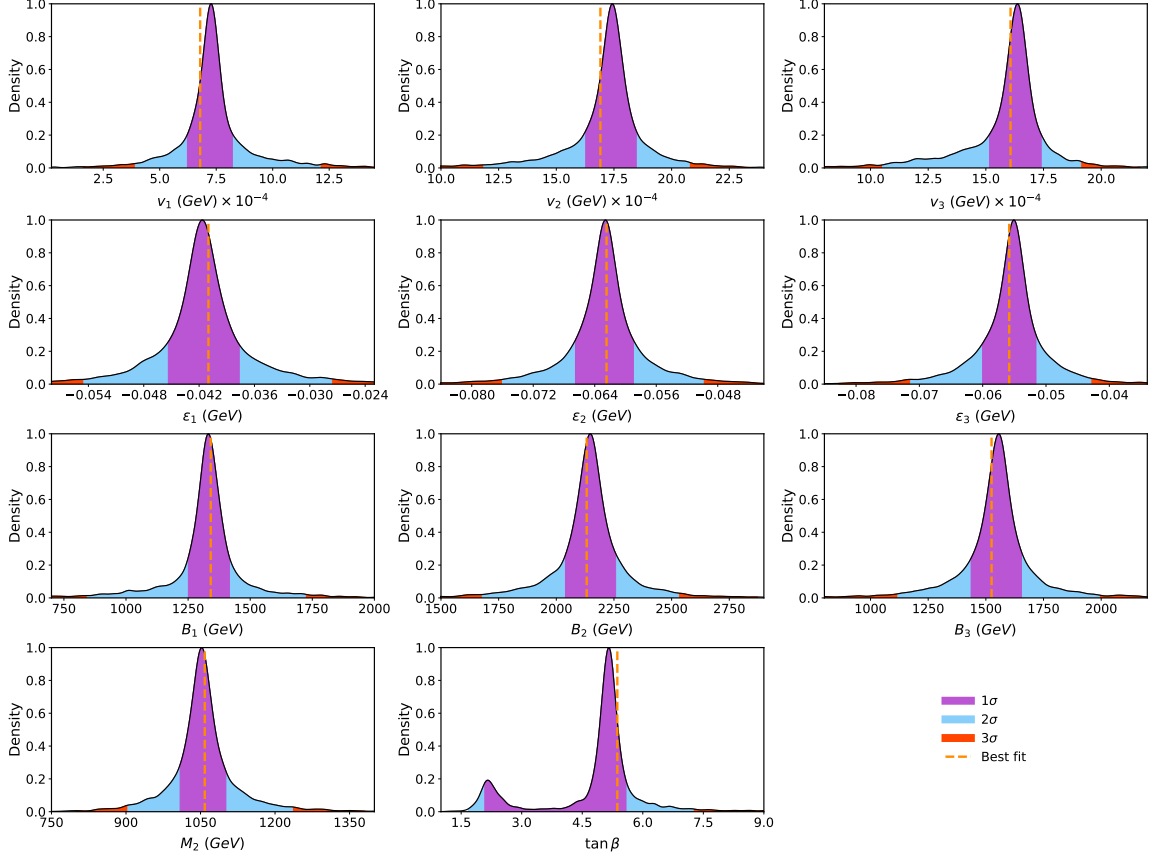


Figure 9: The 1-D posterior distribution of all the input parameters for IH scenario along with 1σ , 2σ and 3σ regions are shown here with purple, cyan and red colors respectively. The best-fit value of each parameter is represented by the dashed orange colored line.

Best-fit Point (BFP)							
Input parameters				$m_{\tilde{\chi}_1^0} = 1102 \text{ GeV}$		$m_{\tilde{\chi}_1^\pm} = 1106 \text{ GeV}$	
Parameter	Value	Parameter	Value	Decay	Br (%)	Decay	Br(%)
M_2 [GeV]	1058.49	ϵ_2 [10^{-2}GeV]	-6.24	$W\bar{e}$	0.16	$W\nu_\mu$	43.99
$\tan\beta$	5.36	ϵ_3 [10^{-2}GeV]	-5.58	$W\mu$	21.46	$h\bar{e}$	0.74
v_1 [10^{-4}GeV]	6.79	B_1 [GeV]	1341	$W\tau$	22.36	$h\mu$	17.12
v_2 [10^{-3}GeV]	1.69	B_2 [GeV]	2131	$h\nu_e$	0.28	$h\tau$	15.57
v_3 [10^{-3}GeV]	1.60	B_3 [GeV]	1524	$h\nu_\mu$	33.10	$Z\bar{e}$	0.08
ϵ_1 [10^{-2}GeV]	-4.09			$h\nu_\tau$	0.02	$Z\mu$	11.02
$\chi_{\min}^2/\text{d.o.f} = 3.94/4 = 0.98$				$Z\nu_\mu$	22.62	$Z\tau$	11.48

Table 5: The input parameters at the best-fit point, along with the masses of the wino-type lightest neutralino and chargino and their respective decay branching ratios, are presented corresponding to IH scenario.

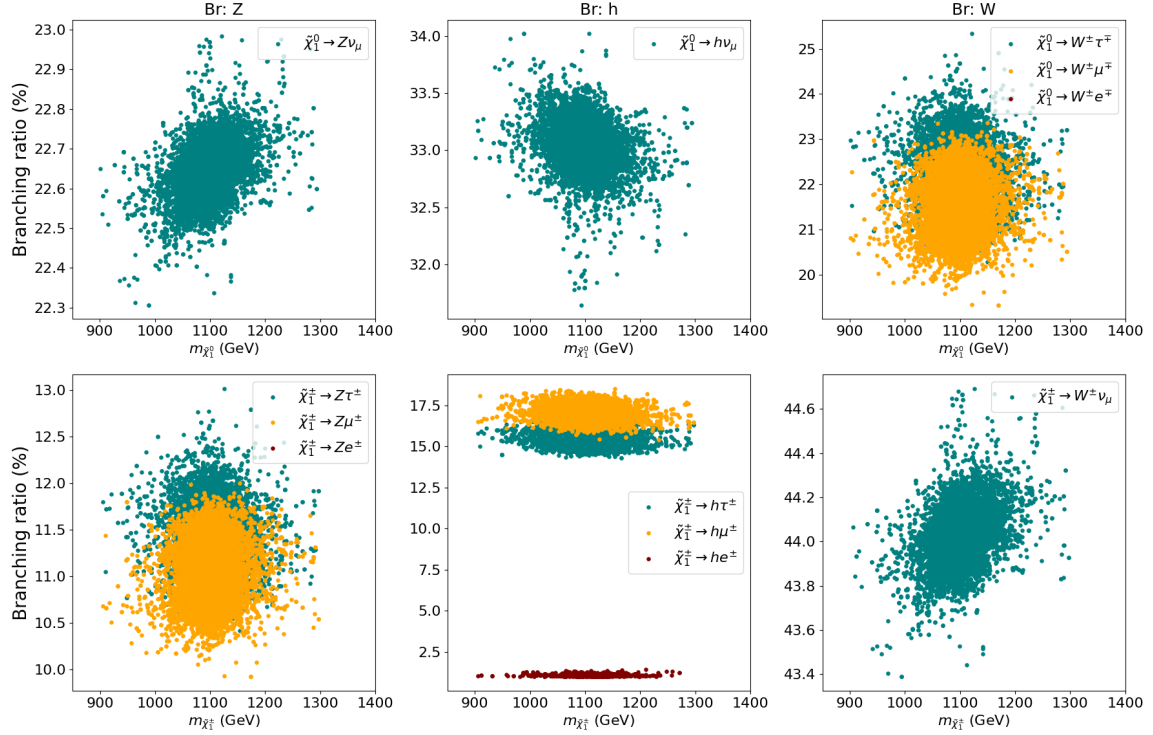


Figure 10: The branching ratios of $\tilde{\chi}_1^0$ and $\tilde{\chi}_1^\pm$ into different lepton flavors are shown. In the upper panel, $\mathcal{B}r(\tilde{\chi}_1^0 \rightarrow Z\nu)$ (left), $\mathcal{B}r(\tilde{\chi}_1^0 \rightarrow h\nu)$ (middle), and $\mathcal{B}r(\tilde{\chi}_1^0 \rightarrow W^\pm l^\mp)$ (right) are presented. In the lower panel, $\mathcal{B}r(\tilde{\chi}_1^\pm \rightarrow Zl^\pm)$ (left), $\mathcal{B}r(\tilde{\chi}_1^\pm \rightarrow hl^\pm)$ (middle), and $\mathcal{B}r(\tilde{\chi}_1^\pm \rightarrow W^\pm \nu)$ (right) are shown. The red, yellow, and teal colors correspond to the first-, second-, and third-generation lepton flavors, respectively.

corresponding to any single flavor must not be very large. This leads to the smaller $\tan\beta$ and M_2 as compared to the NH scenario as shown in Table 5 as well as the allowed regions in Figure 9. The 3σ allowed regions corresponding to $\tan\beta$ and M_2 are 1.5-8.0 and 850-1300 GeV respectively.

The hierarchy of neutrino mass affects the bRPV parameters and controls the pattern of branching ratios of the chargino and neutralino decays into different lepton flavors, as shown in Table 5. The decay branching ratios into different bosons accompanied by a lepton or neutrino are illustrated in Fig. 10. In the IH scenario, the values of the bRPV parameters favor the muon flavor, and therefore the dominant decay channels are $\tilde{\chi}_1^0 \rightarrow Z\nu_\mu$ and $\tilde{\chi}_1^0 \rightarrow h\nu_\mu$, whereas the other two flavors vanish as discussed in the Ref. [70]. Similarly, for the chargino decay $\tilde{\chi}_1^\pm \rightarrow W^\pm \nu_\mu$ becomes the dominant mode.

From Tables 3 and 5, we observe that the total branching ratio $\mathcal{B}r(\tilde{\chi}_1^\pm \rightarrow Zl)$ ($l = e, \mu, \tau$) is approximately 23% for both the NH and IH scenarios. However, the flavor composition of this decay differs significantly between the two cases. For NH,

the decay $\tilde{\chi}_1^\pm \rightarrow Z\tau$ dominates with a branching ratio of about 14%, while $\tilde{\chi}_1^\pm \rightarrow Z\mu$ and $\tilde{\chi}_1^\pm \rightarrow Ze$ each have branching ratios of roughly 4%. In contrast, for the IH, the branching ratios of $\tilde{\chi}_1^\pm \rightarrow Z\tau$ and $\tilde{\chi}_1^\pm \rightarrow Z\mu$ are both around 11%, whereas $\tilde{\chi}_1^\pm \rightarrow Ze$ is highly suppressed. Therefore, although the inclusive $\tilde{\chi}_1^\pm \rightarrow Zl$ rate is similar in the two scenarios, the number of events in flavor-specific channels can differ substantially. In particular, the μ channel is expected to yield significantly more signal events in the IH case than in the NH case. Consequently, flavor-tagged collider searches may provide a means to distinguish between the NH and IH neutrino mass hierarchies.

5 Conclusion

Neutrino oscillation experiments have conclusively demonstrated that the three light neutrinos possess non-zero masses and mix with each other, a feature that the Standard Model (SM) cannot explain. Supersymmetry (SUSY) provides a well-motivated framework for new physics, and in the bilinear R-parity violating (bRPV) SUSY scenario, neutrino masses can be generated naturally without introducing additional particles. In this work, we have investigated neutrino mass generation in the context of bRPV SUSY model. By combining neutrino oscillation data, the observed Higgs mass and its coupling strength modifiers, and flavor physics observables such as B -hadron decay branching ratios, we have conducted an MCMC scan to identify the allowed parameter space for this model parameters while satisfying the current LHC limits. From this allowed region, we selected representative points to illustrate the decay branching ratios of wino-like lighter charginos ($\tilde{\chi}_1^\pm$) and lightest neutralinos ($\tilde{\chi}_1^0$). We find that the branching ratios to different neutrino and charged lepton flavors depend sensitively on the neutrino mass hierarchy. For the Normal Hierarchy scenario, the decay channel producing τ -flavored neutrino together with a SM boson is the dominant mode, whereas in the Inverted Hierarchy case, the decay producing μ -flavored neutrino becomes the dominant one.

Furthermore, we explore the current LHC bounds and future search sensitivity from the trilepton resonance searches on the allowed parameter space. We validate the exclusion limits provided by the ATLAS Collaboration for wino-like $\tilde{\chi}_1^0$ or $\tilde{\chi}_1^\pm$ using trilepton resonance search with Run-II data. We showed that our simulated result has a nice agreement with the experimental limit. Using the branching ratio at the best-fit point $\text{Br}(\tilde{\chi}_1^\pm \rightarrow Zl^\pm) \sim 23\%$, coming from our analysis with neutrino oscillation data along with Higgs data and flavor data, we obtain the current LHC exclusion on the wino-like chargino is around 565 GeV from LHC Run-II data. We also estimate the projected exclusion reach at HL-LHC with $\sqrt{s} = 14$ TeV and $\mathcal{L} = 3$ ab^{-1} . The projected exclusion reach with a similar branching ratio at High-Luminosity LHC (HL-LHC) is around 950 GeV. For the decay of $\tilde{\chi}_1^\pm/\tilde{\chi}_1^0$ into a Z

boson and a lepton with branching ratios of 1%, 50%, and 100%, wino masses can be excluded up to ~ 600 GeV, 1185 GeV, and 1350 GeV respectively. Our analysis shows that the HL-LHC can probe a significant portion of the 1σ allowed parameter space by neutrino oscillation measurements and other experimental constraints. Overall, our results demonstrate the interplay between neutrino physics and collider observables in constraining bRPV SUSY and provide a road-map for testing these scenarios at upcoming experiments.

6 Acknowledgement

AC and AM acknowledge support from the ANRF India through the Core Research Grant No. CRG/2023/008570. The authors are grateful to Subhadeep Mondal and Sourav Mitra for insightful discussions and contributions to the analysis setup. AM thanks Sabine Kraml for her careful reading of the manuscript and constructive comments. AM also acknowledges support from the French Agence Nationale de la Recherche under Grant No. ANR-23-CHRO-0006 (OpenMAPP).

Bibliography

- [1] BOREXINO collaboration, G. Bellini et al., *Final results of Borexino Phase-I on low energy solar neutrino spectroscopy*, *Phys. Rev. D* **89** (2014) 112007, [[1308.0443](#)].
- [2] KAMLAND collaboration, A. Gando et al., *Reactor On-Off Antineutrino Measurement with KamLAND*, *Phys. Rev. D* **88** (2013) 033001, [[1303.4667](#)].
- [3] RENO collaboration, G. Bak et al., *Measurement of Reactor Antineutrino Oscillation Amplitude and Frequency at RENO*, *Phys. Rev. Lett.* **121** (2018) 201801, [[1806.00248](#)].
- [4] DAYA BAY collaboration, D. Adey et al., *Measurement of the Electron Antineutrino Oscillation with 1958 Days of Operation at Daya Bay*, *Phys. Rev. Lett.* **121** (2018) 241805, [[1809.02261](#)].
- [5] SUPER-KAMIOKANDE collaboration, M. Jiang et al., *Atmospheric Neutrino Oscillation Analysis with Improved Event Reconstruction in Super-Kamiokande IV*, *PTEP* **2019** (2019) 053F01, [[1901.03230](#)].
- [6] T2K collaboration, K. Abe et al., *Search for CP Violation in Neutrino and Antineutrino Oscillations by the T2K Experiment with 2.2×10^{21} Protons on Target*, *Phys. Rev. Lett.* **121** (2018) 171802, [[1807.07891](#)].
- [7] NOvA collaboration, M. A. Acero et al., *First Measurement of Neutrino Oscillation Parameters using Neutrinos and Antineutrinos by NOvA*, *Phys. Rev. Lett.* **123** (2019) 151803, [[1906.04907](#)].

- [8] S. Weinberg, *A model of leptons*, *Phys. Rev. Lett.* **19** (Nov, 1967) 1264–1266.
- [9] A. Salam, *Weak and Electromagnetic Interactions*, *Conf. Proc. C* **680519** (1968) 367–377.
- [10] M. Gell-Mann, *A schematic model of baryons and mesons*, *Physics Letters* **8** (1964) 214–215.
- [11] M. Drees, R. Godbole and P. Roy, *Theory and Phenomenology of Sparticles: An Account of Four-Dimensional $N = 1$ Supersymmetry in High Energy Physics*. 01, 2005, [10.1142/4001](https://arxiv.org/abs/10.1142/4001).
- [12] H. Baer and X. Tata, *Weak scale supersymmetry: From superfields to scattering events*. Cambridge University Press, 5, 2006.
- [13] S. P. Martin, *A Supersymmetry primer*, *Adv. Ser. Direct. High Energy Phys.* **18** (1998) 1–98, [[hep-ph/9709356](https://arxiv.org/abs/hep-ph/9709356)].
- [14] L. Susskind, *The gauge hierarchy problem, technicolor, supersymmetry, and all that*, *Physics Reports* **104** (1984) 181–193.
- [15] E. Gildener, *Gauge-symmetry hierarchies*, *Phys. Rev. D* **14** (Sep, 1976) 1667–1672.
- [16] J. Ellis, S. Kelley and D. Nanopoulos, *Precision lep data, supersymmetric guts and string unification*, *Physics Letters B* **249** (1990) 441–448.
- [17] U. Amaldi, W. de Boer and H. Fürstenau, *Comparison of grand unified theories with electroweak and strong coupling constants measured at lep*, *Physics Letters B* **260** (1991) 447–455.
- [18] G. Ross and R. Roberts, *Minimal supersymmetric unification predictions*, *Nuclear Physics B* **377** (1992) 571–592.
- [19] F. Zwicky, *Die Rotverschiebung von extragalaktischen Nebeln*, *Helv. Phys. Acta* **6** (1933) 110–127.
- [20] F. Zwicky, *On the Masses of Nebulae and of Clusters of Nebulae*, *apj* **86** (Oct., 1937) 217.
- [21] Y. Sofue and V. Rubin, *Rotation curves of spiral galaxies*, *Ann. Rev. Astron. Astrophys.* **39** (2001) 137–174, [[astro-ph/0010594](https://arxiv.org/abs/astro-ph/0010594)].
- [22] G. Jungman, M. Kamionkowski and K. Griest, *Supersymmetric dark matter*, *Phys. Rept.* **267** (1996) 195–373, [[hep-ph/9506380](https://arxiv.org/abs/hep-ph/9506380)].
- [23] H. K. Dreiner, *An Introduction to explicit R-parity violation*, *Adv. Ser. Direct. High Energy Phys.* **21** (2010) 565–583, [[hep-ph/9707435](https://arxiv.org/abs/hep-ph/9707435)].
- [24] R. Barbier et al., *R-parity violating supersymmetry*, *Phys. Rept.* **420** (2005) 1–202, [[hep-ph/0406039](https://arxiv.org/abs/hep-ph/0406039)].
- [25] A. Choudhury, A. Mondal and S. Mondal, *Status of R-parity violating SUSY*, *Eur. Phys. J. Spec. Top.* **233** (2024) 2187–2208, [[2402.04040](https://arxiv.org/abs/2402.04040)].

- [26] T. Banks, Y. Grossman, E. Nardi and Y. Nir, *Supersymmetry without R-parity and without lepton number*, *Phys. Rev. D* **52** (1995) 5319–5325, [[hep-ph/9505248](#)].
- [27] Y. Grossman and H. E. Haber, *(S)neutrino properties in R-parity violating supersymmetry. 1. CP conserving phenomena*, *Phys. Rev. D* **59** (1999) 093008, [[hep-ph/9810536](#)].
- [28] S. Davidson and M. Losada, *Neutrino masses in the R(p) violating MSSM*, *JHEP* **05** (2000) 021, [[hep-ph/0005080](#)].
- [29] S. Davidson and M. Losada, *Basis independent neutrino masses in the R(p) violating MSSM*, *Phys. Rev. D* **65** (2002) 075025, [[hep-ph/0010325](#)].
- [30] F. Borzumati, Y. Grossman, E. Nardi and Y. Nir, *Neutrino masses and mixing in supersymmetric models without R parity*, *Phys. Lett. B* **384** (1996) 123–130, [[hep-ph/9606251](#)].
- [31] B. Mukhopadhyaya, S. Roy and F. Vissani, *Correlation between neutrino oscillations and collider signals of supersymmetry in an R-parity violating model*, *Phys. Lett. B* **443** (1998) 191–195, [[hep-ph/9808265](#)].
- [32] S. Rakshit, G. Bhattacharyya and A. Raychaudhuri, *r-parity-violating trilinear couplings and recent neutrino data*, *Phys. Rev. D* **59** (Mar, 1999) 091701.
- [33] A. Datta, B. Mukhopadhyaya and S. Roy, *Constraining an r-parity violating supersymmetric theory from the superkamiokande data on atmospheric neutrinos*, *Phys. Rev. D* **61** (Feb, 2000) 055006.
- [34] B. C. Allanach and C. H. Kom, *Lepton number violating mSUGRA and neutrino masses*, *JHEP* **04** (2008) 081, [[0712.0852](#)].
- [35] B. C. Allanach, C. H. Kom and M. Hanussek, *Computation of Neutrino Masses in R-parity Violating Supersymmetry: SOFTSUSY3.2*, *Comput. Phys. Commun.* **183** (2012) 785–793, [[1109.3735](#)].
- [36] Y. Grossman and H. E. Haber, *Sneutrino mixing phenomena*, *Phys. Rev. Lett.* **78** (1997) 3438–3441, [[hep-ph/9702421](#)].
- [37] H. K. Dreiner and G. G. Ross, *R-parity violation at hadron colliders*, *Nucl. Phys. B* **365** (1991) 597–613.
- [38] D. Dercks, H. Dreiner, M. E. Krauss, T. Opferkuch and A. Reinert, *R-Parity Violation at the LHC*, *Eur. Phys. J. C* **77** (2017) 856, [[1706.09418](#)].
- [39] R. Bose, A. Datta, A. Kundu and S. Poddar, *LHC signatures of neutrino mass generation through R-parity violation*, *Phys. Rev. D* **90** (2014) 035007, [[1405.1282](#)].
- [40] A. Datta and S. Poddar, *Probing R-parity violating models of neutrino mass at the LHC via top squark decays*, *Phys. Rev. D* **79** (2009) 075021, [[0901.1619](#)].
- [41] S. P. Das, A. Datta and S. Poddar, *Top squark and neutralino decays in a R-parity violating model constrained by neutrino oscillation data*, *Phys. Rev. D* **73** (2006) 075014, [[hep-ph/0509171](#)].

- [42] V. A. Mitsou, *R-parity violating supersymmetry and neutrino physics: experimental signatures*, *PoS PLANCK2015* (2015) 085, [[1510.02660](#)].
- [43] J. Cohen, S. Bar-Shalom, G. Eilam and A. Soni, *R -parity violating supersymmetry and the 125 GeV Higgs boson signals*, *Phys. Rev. D* **100** (2019) 115051, [[1906.04743](#)].
- [44] S. Weinberg, *Baryon and Lepton Nonconserving Processes*, *Phys. Rev. Lett.* **43** (1979) 1566–1570.
- [45] S. Weinberg, *Varieties of Baryon and Lepton Nonconservation*, *Phys. Rev. D* **22** (1980) 1694.
- [46] P. Minkowski, *$\mu \rightarrow e\gamma$ at a Rate of One Out of 10^9 Muon Decays?*, *Phys. Lett. B* **67** (1977) 421–428.
- [47] M. Gell-Mann, P. Ramond and R. Slansky, *Complex Spinors and Unified Theories*, *Conf. Proc. C* **790927** (1979) 315–321, [[1306.4669](#)].
- [48] J. Schechter and J. W. F. Valle, *Neutrino Masses in $SU(2) \times U(1)$ Theories*, *Phys. Rev. D* **22** (1980) 2227.
- [49] R. N. Mohapatra and G. Senjanovic, *Neutrino Mass and Spontaneous Parity Nonconservation*, *Phys. Rev. Lett.* **44** (1980) 912.
- [50] J. Schechter and J. W. F. Valle, *Neutrino Decay and Spontaneous Violation of Lepton Number*, *Phys. Rev. D* **25** (1982) 774.
- [51] S. Rakshit, *Neutrino masses and R-parity violation*, *Mod. Phys. Lett. A* **19** (2004) 2239–2258, [[hep-ph/0406168](#)].
- [52] Y. Grossman and S. Rakshit, *Neutrino masses in R-parity violating supersymmetric models*, *Phys. Rev. D* **69** (2004) 093002, [[hep-ph/0311310](#)].
- [53] A. Choudhury, S. Mitra, A. Mondal and S. Mondal, *An MCMC analysis to probe trilinear RPV SUSY scenarios and possible LHC signatures*, [2411.08112](#).
- [54] S. Roy and B. Mukhopadhyaya, *Some implications of a supersymmetric model with R-parity breaking bilinear interactions*, *Phys. Rev. D* **55** (1997) 7020–7029, [[hep-ph/9612447](#)].
- [55] B. de Carlos and P. L. White, *R-parity violation effects through soft supersymmetry breaking terms and the renormalization group*, *Phys. Rev. D* **54** (1996) 3427–3446, [[hep-ph/9602381](#)].
- [56] E. Nardi, *Renormalization group induced neutrino masses in supersymmetry without R-parity*, *Phys. Rev. D* **55** (1997) 5772–5779, [[hep-ph/9610540](#)].
- [57] R. Hempfling, *Neutrino masses and mixing angles in SUSY GUT theories with explicit R-parity breaking*, *Nucl. Phys. B* **478** (1996) 3–30, [[hep-ph/9511288](#)].
- [58] M. Hirsch, M. A. Diaz, W. Porod, J. C. Romao and J. W. F. Valle, *Neutrino masses and mixings from supersymmetry with bilinear R parity violation: A Theory*

- for solar and atmospheric neutrino oscillations, *Phys. Rev. D* **62** (2000) 113008, [[hep-ph/0004115](#)].
- [59] R. S. Hundi, *Constraints from neutrino masses and muon ($g-2$) in the bilinear R -parity violating supersymmetric model*, *Phys. Rev. D* **83** (2011) 115019, [[1101.2810](#)].
- [60] M. A. Díaz, M. Rivera and N. Rojas, *On Neutrino Masses in the MSSM with $BRpV$* , *Nucl. Phys. B* **887** (2014) 338–357, [[1401.7357](#)].
- [61] M. Hirsch, J. C. Romao and J. W. F. Valle, *Bilinear R -parity violating SUSY: Neutrinoless double beta decay in the light of solar and atmospheric neutrino data*, *Phys. Lett. B* **486** (2000) 255–262, [[hep-ph/0002264](#)].
- [62] A. Abada, S. Davidson and M. Losada, *Neutrino masses and mixings in the MSSM with soft bilinear $R(p)$ violation*, *Phys. Rev. D* **65** (2002) 075010, [[hep-ph/0111332](#)].
- [63] M. A. Diaz, C. Mora and A. R. Zerwekh, *Study of a neutrino mass texture generated in supergravity with bilinear R -parity violation*, *Eur. Phys. J. C* **44** (2005) 277–286, [[hep-ph/0410285](#)].
- [64] F. de Campos, O. J. P. Eboli, M. B. Magro, W. Porod, D. Restrepo, S. P. Das et al., *Probing Neutralino Properties in Minimal Supergravity with Bilinear R -Parity Violation*, *Phys. Rev. D* **86** (2012) 075001, [[1206.3605](#)].
- [65] M. Gozdz and W. A. Kaminski, *Constraining bilinear R -parity violation from neutrino masses*, *Phys. Rev. D* **78** (2008) 075021, [[1201.1241](#)].
- [66] A. Choudhury, S. Mitra, A. Mondal and S. Mondal, *Bilinear R -parity violating supersymmetry under the light of neutrino oscillation, Higgs and flavor data*, *JHEP* **02** (2024) 004, [[2305.15211](#)].
- [67] H. K. Dreiner, D. Köhler and S. Nangia, *A ν approach to analyzing neutrino data in the R -parity-violating MSSM*, *Eur. Phys. J. C* **83** (2023) 44, [[2210.07253](#)].
- [68] P. Fileviez Perez and S. Spinner, *The Minimal Theory for R -parity Violation at the LHC*, *JHEP* **04** (2012) 118, [[1201.5923](#)].
- [69] S. Dumitru, B. A. Ovrut and A. Purves, *The R -parity Violating Decays of Charginos and Neutralinos in the B - L MSSM*, *JHEP* **02** (2019) 124, [[1810.11035](#)].
- [70] S. Dumitru, B. A. Ovrut and A. Purves, *R -parity Violating Decays of Wino Chargino and Wino Neutralino LSPs and NLSPs at the LHC*, *JHEP* **06** (2019) 100, [[1811.05581](#)].
- [71] ATLAS collaboration, G. Aad et al., *Search for trilepton resonances from chargino and neutralino pair production in $\sqrt{s} = 13$ TeV pp collisions with the ATLAS detector*, *Phys. Rev. D* **103** (2021) 112003, [[2011.10543](#)].
- [72] A. Collaboration, “Atlas experiment - public results.” <https://twiki.cern.ch/twiki/bin/view/AtlasPublic/SupersymmetryPublicResults>, 2023.

- [73] C. Collaboration, “Cms experiment - physics results.” <https://twiki.cern.ch/twiki/bin/view/CMSPublic/PhysicsResultsSUS>, 2023.
- [74] X. Wang and M. Abdughani, *Current status and prospects of light bino-higgsino dark matter in natural SUSY*, [2602.14088](#).
- [75] L. Constantin, S. Kraml, A. Lessa, T. Reymermier and W. Waltenberger, *On the coverage of electroweak-inos within the pMSSM with SModelS – a comparison with the ATLAS pMSSM study*, [2512.14502](#).
- [76] A. Chatterjee, A. Choudhury, S. Mitra, A. Mondal and S. Mondal, *Exploring the BSM parameter space with neural network aided Simulation-Based Inference*, *JHEP* **12** (2025) 138, [[2502.11928](#)].
- [77] A. Choudhury, A. Mondal and S. Sarkar, *Searches for the BSM scenarios at the LHC using decision tree-based machine learning algorithms: a comparative study and review of random forest, AdaBoost, XGBoost and LightGBM frameworks*, *Eur. Phys. J. ST* **233** (2024) 2425–2463, [[2405.06040](#)].
- [78] A. S. Cornell, B. Fuks, M. D. Goodsell and A. M. Ncube, *Improving smuon searches with neural networks*, *Eur. Phys. J. C* **85** (2025) 51, [[2411.04526](#)].
- [79] M. M. Altakach, S. Kraml, A. Lessa, S. Narasimha, T. Pascal, T. Reymermier et al., *Global LHC constraints on electroweak-inos with SModelS v2.3*, *SciPost Phys.* **16** (2024) 101, [[2312.16635](#)].
- [80] M. Chakraborti, U. Chattopadhyay and S. Poddar, *How light a higgsino or a wino dark matter can become in a compressed scenario of MSSM*, *JHEP* **09** (2017) 064, [[1702.03954](#)].
- [81] S. Bisal, A. Chatterjee, D. Das and S. A. Pasha, *Radiative corrections to the direct detection of the Higgsino- and wino-like neutralino dark matter: Spin-dependent interactions*, *Phys. Rev. D* **111** (2025) 083003, [[2410.18205](#)].
- [82] D. Chowdhury, K. M. Patel, X. Tata and S. K. Vempati, *Indirect Searches of the Degenerate MSSM*, *Phys. Rev. D* **95** (2017) 075025, [[1612.06471](#)].
- [83] R. K. Barman, B. Bhattacharjee, A. Chakraborty and A. Choudhury, *Study of MSSM heavy Higgs bosons decaying into charginos and neutralinos*, *Phys. Rev. D* **94** (2016) 075013, [[1607.00676](#)].
- [84] A. Choudhury and S. Mondal, *Revisiting the Exclusion Limits from Direct Chargino-Neutralino Production at the LHC*, *Phys. Rev. D* **94** (2016) 055024, [[1603.05502](#)].
- [85] M. Chakraborti, U. Chattopadhyay, A. Choudhury, A. Datta and S. Poddar, *Reduced LHC constraints for higgsino-like heavier electroweakinos*, *JHEP* **11** (2015) 050, [[1507.01395](#)].
- [86] M. Chakraborti, U. Chattopadhyay, A. Choudhury, A. Datta and S. Poddar, *The Electroweak Sector of the pMSSM in the Light of LHC - 8 TeV and Other Data*, *JHEP* **07** (2014) 019, [[1404.4841](#)].

- [87] A. Choudhury and A. Datta, *Neutralino dark matter confronted by the LHC constraints on Electroweak SUSY signals*, *JHEP* **09** (2013) 119, [[1305.0928](#)].
- [88] A. Choudhury and A. Datta, *Many faces of low mass neutralino dark matter in the unconstrained MSSM, LHC data and new signals*, *JHEP* **06** (2012) 006, [[1203.4106](#)].
- [89] N. Bhattacharyya, A. Choudhury and A. Datta, *Low mass neutralino dark matter in mSUGRA and more general models in the light of LHC data*, *Phys. Rev. D* **84** (2011) 095006, [[1107.1997](#)].
- [90] R. K. Barman, A. Choudhury and S. Sarkar, *Revisiting the Electroweakino Sector of the Baryon Number Violating MSSM at the HL-LHC with Deep Neural Networks*, [2602.06957](#).
- [91] G. Cottin, J. C. Helo, F. Hernández-Pinto, N. A. Neill and Z. S. Wang, *Probing light neutralinos from pair-produced sleptons with displaced vertices at the high-luminosity LHC*, *JHEP* **09** (2025) 102, [[2505.06365](#)].
- [92] R. Baruah, A. Choudhury, K. Ghosh, S. Mondal and R. Sahu, *Probing sub-TeV Higgsinos aided by a machine-learning-based top tagger in the context of trilinear R-parity violating SUSY*, *Phys. Rev. D* **111** (2025) 095004, [[2412.11862](#)].
- [93] H. K. Dreiner, M. Hank, Y. S. Koay, M. Schürmann, R. Sengupta, A. Shah et al., *The ABC of RPV II: Classification of R-parity Violating Signatures from UDD Couplings and their Coverage at the LHC*, [2503.03830](#).
- [94] A. Choudhury, A. Mondal, S. Mondal and S. Sarkar, *Slepton searches in the trilinear RPV SUSY scenarios at the HL-LHC and HE-LHC*, [2310.07532](#).
- [95] B. Bhattacharjee and P. Solanki, *Search for electroweakinos in R-parity violating SUSY with long-lived particles at HL-LHC*, *JHEP* **12** (2023) 148, [[2308.05804](#)].
- [96] H. K. Dreiner, Y. S. Koay, D. Köhler, V. M. Lozano, J. Montejo Berlingen, S. Nangia et al., *The ABC of RPV: classification of R-parity violating signatures at the LHC for small couplings*, *JHEP* **07** (2023) 215, [[2306.07317](#)].
- [97] A. Choudhury, A. Mondal, S. Mondal and S. Sarkar, *Improving sensitivity of trilinear R-parity violating SUSY searches using machine learning at the LHC*, *Phys. Rev. D* **109** (2024) 035001, [[2308.02697](#)].
- [98] R. K. Barman, B. Bhattacharjee, I. Chakraborty, A. Choudhury and N. Khan, *Electroweakino searches at the HL-LHC in the baryon number violating MSSM*, *Phys. Rev. D* **103** (2021) 015003, [[2003.10920](#)].
- [99] R. K. Barman, A. Choudhury and S. Sarkar, *Reconstructing Sparticle masses at the LHC using Generative Machine Learning*, [2507.20869](#).
- [100] E. J. Chun, D.-W. Jung and J. D. Park, *Bi-large neutrino mixing from bilinear R-parity violation with non-universality*, *Phys. Lett. B* **557** (2003) 233–239, [[hep-ph/0211310](#)].

- [101] Y. Grossman and H. E. Haber, *Basis independent analysis of the sneutrino sector in R-parity violating supersymmetry*, *Phys. Rev. D* **63** (2001) 075011, [[hep-ph/0005276](#)].
- [102] P. F. de Salas, D. V. Forero, S. Gariazzo, P. Martínez-Miravé, O. Mena, C. A. Ternes et al., *2020 global reassessment of the neutrino oscillation picture*, *JHEP* **02** (2021) 071, [[2006.11237](#)].
- [103] B. C. Allanach, A. Djouadi, J. L. Kneur, W. Porod and P. Slavich, *Precise determination of the neutral Higgs boson masses in the MSSM*, *JHEP* **09** (2004) 044, [[hep-ph/0406166](#)].
- [104] C. Collaboration, “Cms analysis physics summary.” <https://cds.cern.ch/record/2706103/files/HIG-19-005-pas.pdf>, 2019.
- [105] LHCb collaboration, R. Aaij et al., *Analysis of Neutral B-Meson Decays into Two Muons*, *Phys. Rev. Lett.* **128** (2022) 041801, [[2108.09284](#)].
- [106] HFLAV collaboration, Y. S. Amhis et al., *Averages of b-hadron, c-hadron, and τ -lepton properties as of 2018*, *Eur. Phys. J. C* **81** (2021) 226, [[1909.12524](#)].
- [107] PLANCK collaboration, N. Aghanim et al., *Planck 2018 results. VI. Cosmological parameters*, *Astron. Astrophys.* **641** (2020) A6, [[1807.06209](#)].
- [108] ATLAS collaboration, G. Aad et al., *Search for supersymmetry in events with four or more charged leptons in 139 fb⁻¹ of $\sqrt{s} = 13$ TeV pp collisions with the ATLAS detector*, *JHEP* **07** (2021) 167, [[2103.11684](#)].
- [109] CMS collaboration, V. Khachatryan et al., *Searches for R-parity-violating supersymmetry in ppcollisions at $\sqrt{s} = 8$ TeV in final states with 0-4 leptons*, *Phys. Rev. D* **94** (2016) 112009, [[1606.08076](#)].
- [110] CMS collaboration, S. Chatrchyan et al., *Search for Top Squarks in R-Parity-Violating Supersymmetry using Three or More Leptons and B-Tagged Jets*, *Phys. Rev. Lett.* **111** (2013) 221801, [[1306.6643](#)].
- [111] ATLAS collaboration, G. Aad et al., *Search for direct production of winos and higgsinos in events with two same-charge leptons or three leptons in pp collision data at $\sqrt{s} = 13$ TeV with the ATLAS detector*, *JHEP* **11** (2023) 150, [[2305.09322](#)].
- [112] ATLAS collaboration, M. Aaboud et al., *Search for B-L R -parity-violating top squarks in $\sqrt{s} = 13$ TeV pp collisions with the ATLAS experiment*, *Phys. Rev. D* **97** (2018) 032003, [[1710.05544](#)].
- [113] ATLAS collaboration, G. Aad et al., *A search for R-parity violating supersymmetric decays of the top squark to a b-jet and a lepton in $\sqrt{s} = 13$ TeV pp collisions with the ATLAS detector*, [2406.18367](#).
- [114] CMS collaboration, A. M. Sirunyan et al., *Search for additional neutral MSSM Higgs bosons in the $\tau\tau$ final state in proton-proton collisions at $\sqrt{s} = 13$ TeV*, *JHEP* **09** (2018) 007, [[1803.06553](#)].

- [115] ATLAS collaboration, G. Aad et al., *Search for heavy Higgs bosons decaying into two tau leptons with the ATLAS detector using pp collisions at $\sqrt{s} = 13$ TeV*, *Phys. Rev. Lett.* **125** (2020) 051801, [[2002.12223](#)].
- [116] F. Staub, *SARAH*, [0806.0538](#).
- [117] F. Staub, *Automatic Calculation of supersymmetric Renormalization Group Equations and Self Energies*, *Comput. Phys. Commun.* **182** (2011) 808–833, [[1002.0840](#)].
- [118] F. Staub, *Exploring new models in all detail with SARAH*, *Adv. High Energy Phys.* **2015** (2015) 840780, [[1503.04200](#)].
- [119] W. Porod, *SPheno, a program for calculating supersymmetric spectra, SUSY particle decays and SUSY particle production at e^+e^- colliders*, *Comput. Phys. Commun.* **153** (2003) 275–315, [[hep-ph/0301101](#)].
- [120] W. Porod and F. Staub, *SPheno 3.1: Extensions including flavour, CP-phases and models beyond the MSSM*, *Comput. Phys. Commun.* **183** (2012) 2458–2469, [[1104.1573](#)].
- [121] W. Porod, F. Staub and A. Vicente, *A Flavor Kit for BSM models*, *Eur. Phys. J. C* **74** (2014) 2992, [[1405.1434](#)].
- [122] D. Foreman-Mackey, D. W. Hogg, D. Lang and J. Goodman, *emcee: the mcmc hammer*, *Publications of the Astronomical Society of the Pacific* **125** (2013) 306.
- [123] PARTICLE DATA GROUP collaboration, R. L. Workman et al., *Review of Particle Physics*, *PTEP* **2022** (2022) 083C01.
- [124] A. Collaboration, “Auxiliary material of arxiv:2011.10543 [hep-ex].” <http://atlas.web.cern.ch/Atlas/GROUPS/PHYSICS/PAPERS/SUSY-2018-36>, 2021.
- [125] J. Alwall, R. Frederix, S. Frixione, V. Hirschi, F. Maltoni, O. Mattelaer et al., *The automated computation of tree-level and next-to-leading order differential cross sections, and their matching to parton shower simulations*, *JHEP* **07** (2014) 079, [[1405.0301](#)].
- [126] DELPHES 3 collaboration, J. de Favereau, C. Delaere, P. Demin, A. Giammanco, V. Lemaître, A. Mertens et al., *DELPHES 3, A modular framework for fast simulation of a generic collider experiment*, *JHEP* **02** (2014) 057, [[1307.6346](#)].
- [127] B. Fuks, M. Klasen, D. R. Lamprea and M. Rothering, *Gaugino production in proton-proton collisions at a center-of-mass energy of 8 TeV*, *JHEP* **10** (2012) 081, [[1207.2159](#)].
- [128] B. Fuks, M. Klasen, D. R. Lamprea and M. Rothering, *Precision predictions for electroweak superpartner production at hadron colliders with Resummino*, *Eur. Phys. J. C* **73** (2013) 2480, [[1304.0790](#)].